ACS APPLIED MATERIALS & INTERFACES

Research Article

Cite This: ACS Appl. Mater. Interfaces 2019, 11, 30919−30926

www.acsami.org

Design Strategies to Enhance Amidoxime Chelators for Uranium Recovery

Briana Aguila,[†] Qi Sun,[†] Harper Cassady,[†] Carter W. Abney,[‡] Baiyan Li,[†] and Shengqian Ma*[,†]

[†]Department of Chemistry, University of South Florida, 4202 E Fowler Avenue, Tampa, Florida 33620, United States

[‡]ExxonMobil Research and Engineering Company, 1545 Route 22 East, Annandale, New Jersey 08801, United States

Supporting Information

ABSTRACT: To move nuclear as a primary energy source, uranium resources must be secured beyond what terrestrial reserves can provide. Given the vast quantity of uranium naturally found in the ocean, adsorbent materials have been investigated to recover this vital fuel source. Amidoxime (AO) has been found to be the state-of-the-art functional group for this purpose, however, improvements must still be made to overcome the issues with selectively capturing uranium at such a low concentration found in the ocean. Herein, we report PAF-1 as a platform to study the effects of two amidoxime ligands. The synthesized adsorbents, PAF-1-CH_2NHAO and PAF-1-NH$(CH_2)_2$AO, with varying chain lengths and grafting degrees, were investigated for their uranium uptakes and kinetic efficiency. PAF-1-NH$(CH_2)_2$AO was found to outperform PAF-1-CH_2NHAO, with a maximum uptake capacity of 385 mg/g and able to reduce a uranium-spiked solution to ppb level within 10 min. Further studies with PAF-1-NH$(CH_2)_2$AO demonstrated effective elution for multiple adsorption cycles and showed promising results for uranium recovery in the diverse composition of a spiked seawater solution. The work presented here moves forward design principles for amidoxime-functionalized ligands and provides scope for strategies to enhance the capture of uranium as a sustainable nuclear fuel source.

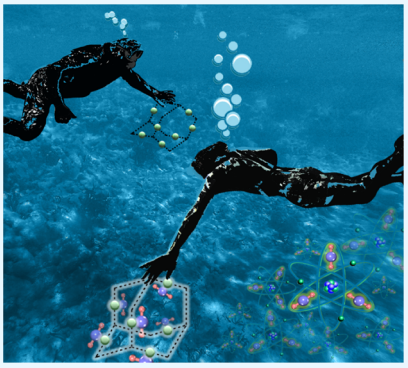

KEYWORDS: *ligand design, nuclear fuel source, porous aromatic framework, selective recovery, uranium capture*

INTRODUCTION

The use of uranium as a fuel source has always carried with it a certain stigma, owing to its radioactivity and popular association with nuclear warfare. This has not prevented the steady progress made in assuring nuclear energy as an alternative to carbon-based fuel.[1−3] Although changing society's perception of the element will be based on its safe and prolonged use and economic validity, overcoming the barriers associated with obtaining uranium in the necessary large quantities is currently becoming more and more attainable. It is well known that the natural ground ores of uranium provide limited resources if we want to utilize nuclear fuel as a sustainable energy source.[4] This has led to the investigation of a nontraditional source of uranium: the ocean.[5−11] Although present in minute quantities, ∼3.3 ppb, the vast supply of oceanic water along with uranium's natural equilibrium makes this a viable source for a potentially renewable energy resource.[12] However, this is all contingent on the ability to recover uranium at a price point that can compete with traditional energy supplies.[13,14]

Previous approaches to isolate uranium are heavily reliant on chemical separations to sequester from complex mixtures. However, chemical processes, such as coagulation and co-precipitation, are difficult to manage for extremely large volumes and result in energy-intensive and costly methods.[12] Adsorbents have been recognized as ideal due to their heterogeneity, able to remove target analytes in the liquid phase with simple filtration required for separation and recovery.[15] Many adsorbent materials have been investigated for this purpose, including carbonaceous materials,[16,17] graphene oxides,[18,19] grafted fibers,[20,21] metal−organic frameworks (MOFs),[22,23] and layered metal sulfides.[24,25] However, their performance is noticeably hindered due to low stability, low degree of functionality, and/or low surface area. These issues must be addressed to achieve high selectivity and uptake for recovery from the ocean's diverse composition. Porous organic polymers (POPs) have emerged as a cutting-edge material formed from strong covalent bonds.[26−31] This class of material combines the advantages of tunable, advanced structures, such as MOFs,[32,33] with the stability of traditional materials, such as activated carbon.[34] This type of material demonstrates all of the features required for such a challenging adsorption process.

Our research group has investigated a variety of POP platforms for the capture of analytes at the interface of the solid and aqueous phases. One such POP that has demonstrated success in water treatment and resource recovery has been PAF-1 (porous aromatic framework).[35−38] The strong covalent bonds provide high stability in a range of conditions, and the aromatic rings can be easily functionalized

Received: May 31, 2019
Accepted: August 4, 2019
Published: August 5, 2019

DOI: 10.1021/acsami.9b09532
ACS Appl. Mater. Interfaces 2019, 11, 30919−30926

Scheme 1. PAF-1 as a Platform to Design Adsorbents with Varying Amidoxime Functionalities for the Capture of Uranium

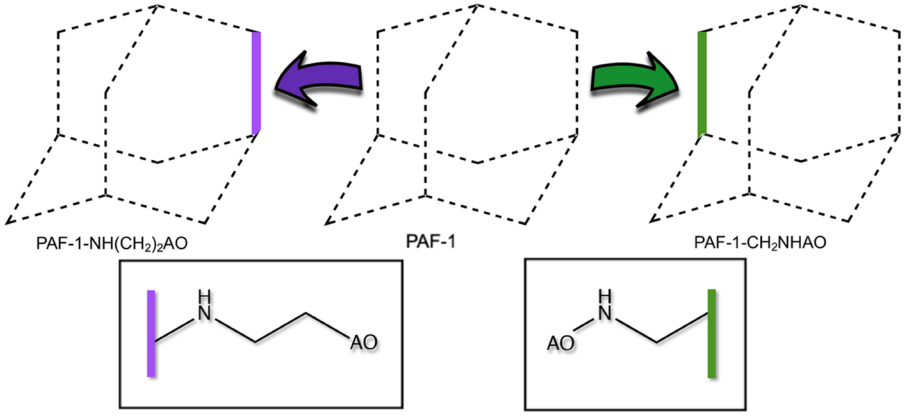

with a high degree of grafting. Promising results with ion exchange for the precious metal capture[39] and strong coordination for mercury removal[40] led to the exploration of this platform for uranium recovery. To target the uranyl ions found in the solution, an amidoxime group ($-C(NOH)NH_2$) was grafted onto PAF-1 through post-synthetic modification with very encouraging results. The subsequent material, PAF-1-CH_2AO (where AO represents the amidoxime group), had an uptake capacity over 300 mg/g and was able to lower a uranyl solution of 4.1 ppm to less than 1.0 ppb after 90 min of treatment, establishing the success of PAF-1 as a platform for recovery of uranium.[41]

Amidoxime has proven itself as the state-of-the-art functional group for uranium recovery;[12,42−45] however, improvements can still be made to optimize the performance of this functionality. Open-chain amidoxime typically binds to uranyl ions in an η^2 coordination manner in the equatorial plane;[46−48] therefore, it is beneficial to have a high content of functional groups to enhance potential cooperation for strong binding and high uptakes.[12] Such a scope for the design of the ligand will result in an adsorbent that can be applied for efficient recovery of uranium from seawater. Herein, we utilize PAF-1 as a stable and easily functionalizable platform to study the effects of two adsorbents with varying amidoxime ligands, denoted as PAF-1-CH_2NHAO and PAF-1-$NH(CH_2)_2$AO. The analysis focused on their grafting degree, flexibility, and cooperation for uranium recovery. This work highlights the variability of a functional group and the strategies that can be taken to enhance adsorbents for real-world applications.

EXPERIMENTAL SECTION

Reagents and Materials. All reagents were commercially available and purchased in high purity with no further purification required. Ultrapure water was obtained through a Millipore water purification system.

Synthesis. *Amidoximation Procedure.* The cyano-functionalized PAF adsorbents were treated with a solution of hydroxylamine and potassium carbonate in ethanol. When stirring in a Schlenk tube, the reaction was heated to 75 °C for 72 h. The tube was cooled naturally to room temperature, and the solids were collected by filtration and subsequently washed with excess water before drying under vacuum to produce the final amidoxime-functionalized PAF materials, PAF-1-CH_2NHAO and PAF-1-$NH(CH_2)_2$AO (Scheme 1).

Base Treatment. All adsorbent materials were base-treated to deprotonate the amidoxime group, which leads to enhanced uranium uptake (Figure S1). The adsorbents were treated with a 3 wt % potassium hydroxide solution for 24 h. Following this, the adsorbents were filtered, washed with water, and dried under vacuum prior to uranium adsorption experiments.

Instrumentation. Fourier-transform infrared (FT-IR) spectra were recorded on a Nicolet Impact 410 FT-IR spectrometer. ^{13}C (100.5 MHz) cross-polarization magic angle spinning data was recorded on a Varian infinity plus 400 spectrometer equipped with a magic angle spin probe in a 4 mm ZrO_2 rotor. Nitrogen sorption isotherms were collected on an ASAP 2020 surface area analyzer. Measurements were taken at 77 K with a liquid nitrogen bath, and the surface areas were calculated using the Brunauer−Emmett−Teller (BET) method. Scanning electron microscopy (SEM) images and energy-dispersive X-ray spectroscopy (EDX) mapping were collected using a Hitachi SU 8000. CHN elemental analysis was performed on a PerkinElmer series II CHN analyzer 2400. Inductively coupled plasma-optical emission spectroscopy (ICP-OES) was performed on a PerkinElmer Elan DRC II Quadrupole. Inductively coupled plasma mass spectrometry (ICP-MS) was performed on an Agilent 7500cx. X-ray photoelectron spectroscopy (XPS) was performed on a Thermo ESCALAB 250 with Al Kα irradiation at $\theta = 90°$ for X-ray sources, and the binding energies were calibrated using the C 1s peak at 285.4 eV. Details of X-ray absorption fine structure (XAFS) spectroscopy studies are listed in the Supporting Information.

Experimental Conditions. A 400 ppm uranium stock solution was made by dissolving 0.5218 g of $UO_2(NO_3)_2{\cdot}6H_2O$ in 500 mL of deionized water. Dilutions of the stock solution with deionized water were performed to obtain lower concentration solutions. Unless otherwise noted, the pH levels of all solutions were adjusted to 6.0 by aqueous solutions of HNO_3 or NaOH. All of the adsorption experiments were performed at ambient conditions.

Uranium Sorption Isotherm. To obtain the adsorption isotherm, 5 mg of the adsorbent was placed in 10 mL of aqueous solutions of increasing uranium concentrations (1−400 ppm). After the solutions were stirred for 24 h, they were filtered through a 0.45 μm membrane filter, and the filtrate was analyzed via ICP to determine the residual uranium concentrations. The amount adsorbed or uptake capacity, q_e (mg/g), at equilibrium was calculated using eq 1

$$q_e = \frac{(C_0 - C_e) \times V}{m} \quad (1)$$

where C_0 and C_e are the initial and equilibrium concentrations, respectively, V is the volume of the solution used (mL), and m is the mass of the adsorbent (g).

Uranium Sorption Kinetics. The adsorbent (5 mg) was added to an Erlenmeyer flask containing 100 mL of a ∼5 ppm uranium solution. The mixture was sonicated for full dispersion and then stirred for 24 h. At increasing time intervals, 3 mL aliquots were removed from the mixture, filtered through a 0.45 μm membrane filter, and the filtrate was analyzed by ICP for the remaining uranium concentration. The kinetic data was fit with the pseudo-second-order kinetic model using eq 2

DOI: 10.1021/acsami.9b09532
ACS Appl. Mater. Interfaces 2019, 11, 30919−30926

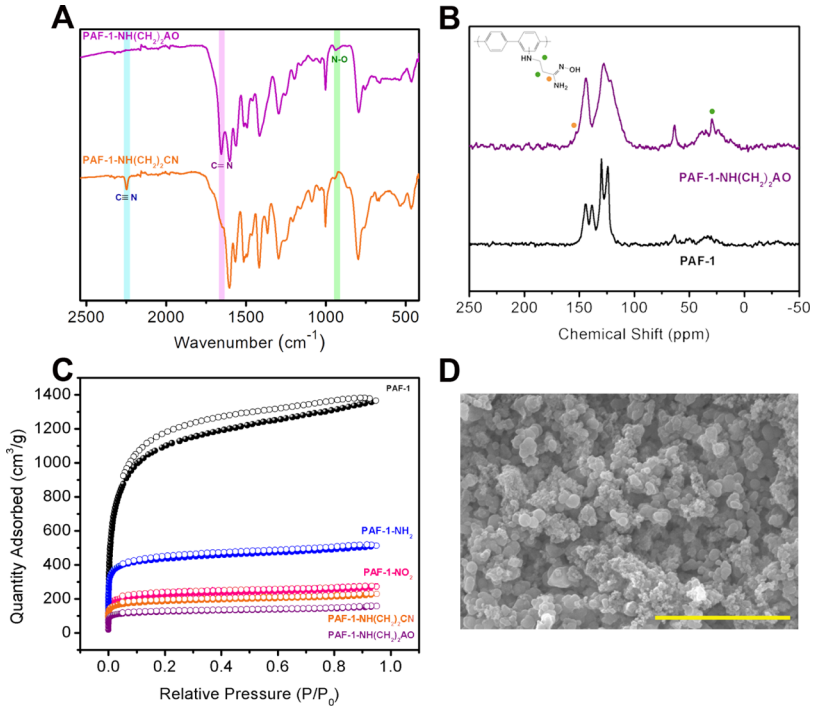

Figure 1. (A) FT-IR spectra; (B) solid-state ^{13}C NMR spectra; (C) nitrogen sorption isotherms; (D) SEM image of PAF-1-NH$(CH_2)_2$AO (scale bar is 5 μm).

$$\frac{t}{q_t} = \frac{1}{k_2 q_e^2} + \frac{t}{q_e} \quad (2)$$

where k_2 is the adsorption rate constant (g/(mg min)), t is the time (min), and q_t and q_e are the uptake capacities (mg/g) at the time (t) and equilibrium, respectively.

Binding Affinity. The adsorbent (2.5 mg) was added to an Erlenmeyer flask containing 100 mL of a 1 ppm uranium solution. The mixture was sonicated for full dispersion and then stirred for 24 h. At increasing time intervals, 3 mL aliquots were removed from the mixture, filtered through a 0.45 μm membrane filter, and the filtrate was analyzed by ICP for the remaining uranium concentration. The distribution coefficient, K_d (mL/g), was calculated using eq 3 based on the residual uranium concentration after 24 h

$$K_d = \frac{(C_0 - C_e)}{C_e} \times \frac{V}{m} \quad (3)$$

where C_0 and C_e are the initial and equilibrium concentrations, respectively, V is the volume of the solution used (mL), and m is the mass of the adsorbent (g).

Elution and Recycling Test. The uranium-contacted adsorbent (20 mg) was stirred in a 1 M Na_2CO_3 solution (100 mL) overnight to elute the uranium from the adsorbent material. The solid was collected by filtration, washed with deionized water, and dried under vacuum for further use. Subsequent adsorption experiments were performed after base treatment and contacted with a 10 ppm uranium solution at a phase ratio of 40 mL/mg.

Spiked Seawater Adsorption. Filtered seawater was collected off the coast of Broad Key, FL. Adsorption experiments were performed at ambient temperature (23 ± 2 °C) and a pH of 8.1. The adsorbent (15 mg) was added to a flask containing 750 mL of the seawater sample spiked with ~8 ppm uranium. The mixture was allowed to stir for 7 days and then filtered through a 0.45 μm membrane filter, and the filtrate was analyzed by ICP for the remaining concentration of metals in solution.

RESULTS AND DISCUSSION

Characterization. After synthesis of the polymeric materials (Schemes S1 and S2), full characterization was performed to understand the physical and chemical properties of the adsorbents. The characterization of PAF-1-NH-$(CH_2)_2$AO will be given as the model adsorbent, with all data for PAF-1-CH_2NHAO provided in the Supplementary Information (Figures S2–S5). Throughout the post-synthetic modification process, the functional groups were tracked by Fourier-transform infrared (FT-IR) spectroscopy (Figure S6). Specifically, the conversion of the cyano group to the amidoxime group was confirmed, with the −CN group having a distinct peak at 2251 cm^{-1} as seen in Figure 1A, after treatment with hydroxylamine, this peak has completely disappeared with the characteristic peaks for amidoxime at 1660 (C═N) and 937 (N−O) cm^{-1} now visible in the spectrum, verifying the complete transformation. Solid-state ^{13}C NMR monitored the carbon chemical shifts of the amidoxime functional group. The alkyl carbons of the extended chain appear at 29 ppm (Figure 1B), as well as a shoulder at 154 ppm representing the carbon of amidoxime, which altogether confirms the grafting and final conversion to amidoxime.[49] To ensure permanent porosity throughout the post-synthetic modification process, nitrogen sorption isotherms were collected at 77 K, and the Brunauer–Emmett–Teller (BET) surface area was calculated for each intermediate. The surface areas changed accordingly with the bulkiness of the functionality, as is the natural trend for porous materials with an increase in weight and a decrease in the available pore volume.[50] Compared to the pristine PAF-1 sample with a BET surface area of 3942 m^2/g, the final material, PAF-1-NH$(CH_2)_2$AO, had a calculated surface area of 465 m^2/g (Figure 1C). Scanning electron microscopy (SEM) was performed to collect nanoscale images of the functionalized adsorbents. From this, the morphology indicated that the

DOI: 10.1021/acsami.9b09532
ACS Appl. Mater. Interfaces 2019, 11, 30919–30926

particles formed irregular aggregates, typical of amorphous solids (Figure 1D). To quantify the addition of the amidoxime functionality, the elemental analysis was utilized, with a N wt % of 14.15% corresponding to an amidoxime content of 3.37 mmol/g. Comparing this to PAF-1-CH_2NHAO with a N wt % of 6.9% corresponding to an amidoxime content of 1.64 mmol/g, it is expected that a higher degree of grafting will enhance the gravimetric performance of the solid adsorbents.

Uranium Adsorption Studies. To test the ligand effects on uranium capture, preliminary experiments were performed to determine the uranium uptake capacity and the kinetic efficiency of both adsorbents. For the maximum uptake capacity, solutions of increasing uranium concentration were treated with the adsorbents. To analyze the equilibrium parameters, the solutions were treated overnight, and the residual uranium concentrations were quantified with inductively coupled plasma-optical emission spectroscopy or mass spectrometry (ICP-OES/MS) (Figure 2A). The

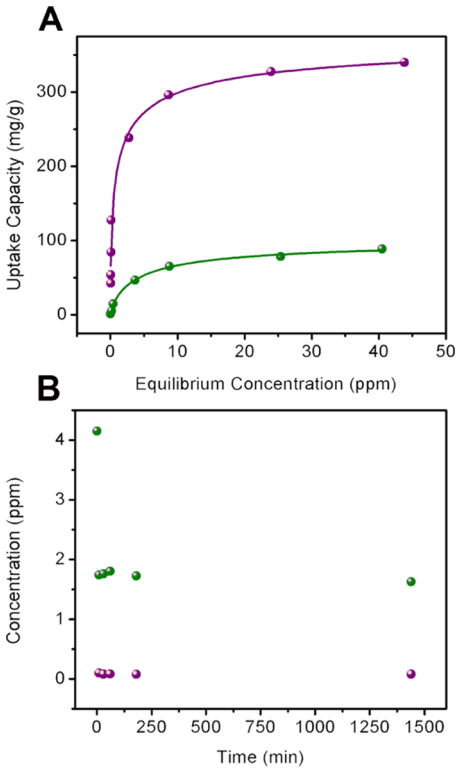

Figure 2. Uranium adsorption performance of PAF-1-$NH(CH_2)_2$AO (purple) and PAF-1-CH_2NHAO (green). (A) Adsorption isotherms (initial uranium concentrations of 1−400 ppm, V/m ratio of 2000 mL/g, pH 6.0); (B) kinetic profile (initial uranium concentration of 4.15 ppm, V/m ratio of 20 000 mL/g, pH 6.0).

adsorption data were fit with the Langmuir model (Figures S7 and S8) with q_{max} values of 102 and 385 mg/g for PAF-1-CH_2NHAO and PAF-1-$NH(CH_2)_2$AO, respectively. This indicates that both adsorbents capture uranium via a monolayer adsorption process,[51] with PAF-1-$NH(CH_2)_2$AO having an almost 4-fold increase over PAF-1- CH_2NHAO. With regard to kinetics, the adsorbents were stirred in a 5 ppm solution of uranium, and aliquots were quantified over time. When analyzing the kinetic profile, both adsorbents demonstrate fast kinetics to reach their maximum adsorption (Figure 2B) and follow the pseudo-second-order kinetic model (Figures S9 and S10). However, PAF-1-$NH(CH_2)_2$AO is able to reduce the uranium to a much lower concentration (0.08 ppm) when compared to PAF-1-CH_2NHAO (1.63 ppm). Given that both adsorbents have amidoxime as their binding site, as well as the fact that PAF-1-CH_2NHAO actually has a higher surface area than PAF-1-$NH(CH_2)_2$AO, it is presumed that the difference in performance is due to the increased flexibility of the PAF-1-$NH(CH_2)_2$AO ligand along with the higher grafting degree. These combined factors allow for an increase in cooperation between ligands for enhanced uranium uptake.

With such encouraging results for PAF-1-$NH(CH_2)_2$AO on both fronts, this adsorbent was chosen for in-depth studies. The previous kinetics demonstrated that the adsorbent could rapidly reduce the uranium concentration to below ppm level, indicating strong binding with the uranyl ions in the solution. This assumption was confirmed by analyzing the binding affinity of the adsorbent with uranium. A 1000 ppb solution of uranium was, thus, treated with the adsorbent, and aliquots were removed over increasing time intervals. Exact concentrations were then quantified with ICP-MS down to ppb level. The uranium concentration rapidly drops, removing nearly 99% of the uranium in the solution within 10 min, and after 16 h, the residual concentration was 1.74 ppb (Figure 3A), which

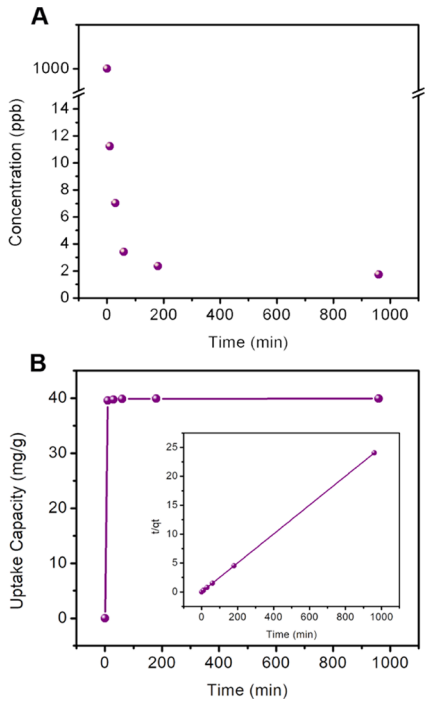

Figure 3. (A) Uranium adsorption kinetics of PAF-1-$NH(CH_2)_2$AO with an initial uranium concentration of 1000 ppb, a phase ratio of 40 000 mL/g, and pH 6.0; (B) kinetic data fit with the pseudo-second order model with a $R^2 = 1$.

fit well with the pseudo-second-order kinetic model (Figure 3B). This equilibrium data was used to calculate the distribution coefficient (K_d), an important metric for determining the affinity of an adsorbent for selected contaminants.[52] Under these conditions, PAF-1-$NH(CH_2)_2$AO had a K_d value of 1.15×10^7 mL/g, indicating an exceptional affinity for uranium. It is worthy to mention that this is an order of magnitude higher than our previous work using a PAF-1-based adsorbent,[41] signifying the importance of

DOI: 10.1021/acsami.9b09532
ACS Appl. Mater. Interfaces 2019, 11, 30919−30926

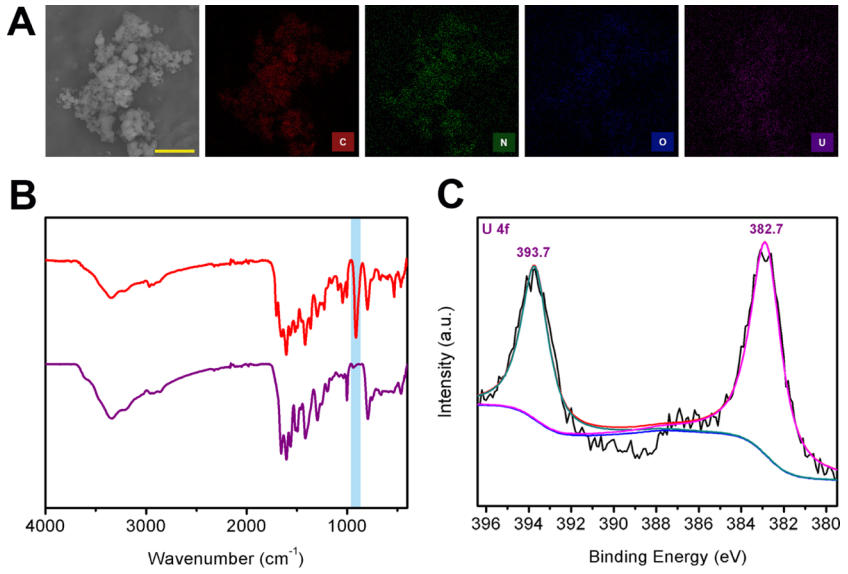

Figure 4. Uranium-contacted PAF-1-NH$(CH_2)_2$AO: (A) SEM image and EDX mapping (scale bar is 5 μm); (B) FT-IR spectra before (purple) and after (red) uranium adsorption; (c) U 4f XPS spectrum.

the design of the ligand for improving a material's ability to capture uranium.

The process of capturing uranium is only the first step in using it as a nuclear fuel source. The uranium must also be eluted from the adsorbent effectively for it to be fully utilized while also regenerating the adsorbent for multiple capture cycles. Rather than using harsh acid treatments to strip the uranium,[21,23,53−55] in this work, we are able to recover the uranium from the adsorbent using a simple treatment with a sodium carbonate solution. This easy process could be expanded on a large scale with minimal environmental impact. Further, the regenerated PAF-1-NH$(CH_2)_2$AO was able to maintain its capacity with near complete recovery and an uptake of 356.6 mg/g after three regeneration cycles (Figure S11). This regenerative ability is comparable or better than other amidoxime materials,[41,56−58] while remaining environmentally benign. This indicates the potential of this adsorbent to be used for repetitive cycles of uranium capture and elution.

With such promising results for the capture of uranium, PAF-1-NH$(CH_2)_2$AO was tested under seawater conditions. One challenge in the adsorption of uranium from seawater is the diverse composition of the water with many ions in extreme excess of the uranium naturally found. To determine the selectivity, a solution of filtered seawater was spiked with ~8 ppm of uranium. PAF-1-NH$(CH_2)_2$AO was introduced into the spiked seawater and allowed to adsorb for 1 week, after which was quantified for its uranium content, along with competing ions, vanadium and iron. PAF-1-NH$(CH_2)_2$AO was found to adsorb 36.5 mg/g of uranium wherein the amount of vanadium adsorbed was only 0.15 μg/g, and the iron concentration was immeasurably low. This uptake capacity is comparable to previously reported materials while also overcoming a major hurdle in seawater adsorption.[24,59] Progresses in material design are vital to address the challenges associated with adsorbing uranium in real seawater conditions, which will involve increasing the binding affinity and selectivity for uranium over the vast number of ions present in much higher concentrations. Modifying ligands is a promising strategy to understand the factors associated with enhanced performance.

Binding Interaction. To understand the binding interaction between the uranyl ions and the adsorbents, we collected EDX mapping images, FT-IR spectra, XPS spectra, and extended XAFS (EXAFS) spectroscopy. As evidenced by EDX images, the uranium is homogeneously distributed throughout PAF-1-CH_2NHAO and PAF-1-NH$(CH_2)_2$AO (Figures S12 and 4A), confirming the adsorption of uranium indicated by the experimental data. The binding between uranyl and the adsorbents was then investigated by FT-IR. When comparing to the spectrum of uranyl nitrate, which has a distinct peak at 935 cm^{-1} corresponding to the asymmetric stretch of O ═ U═O (Figure S13),[60] the spectra for the uranium-contacted adsorbents have an obvious shift to ~904 cm^{-1} (Figures S14 and 4B). This red shift for the peak associated with uranyl is indicative of strong binding between it and the adsorbents. This interaction was further probed through XPS with the appearance of U 4f peaks at 393.7 ($4f_{5/2}$) and 382.7 eV ($4f_{7/2}$) for PAF-1-NH$(CH_2)_2$AO (Figure 4C), with PAF-1-CH_2NHAO having nearly identical peaks (Figure S15). These binding energies are considerably lower than those for pristine uranyl nitrate with peaks at 394.3 and 383.4 eV (Figure S16).[61] The binding between uranyl and the amidoxime functionalities is responsible for the decrease in energy, typical of a metal species after interaction with an electron donor.[62] From these results, we can infer that both adsorbents have moderate to strong binding with uranium.

The uranium−amidoxime coordination environment for both adsorbents was further elucidated using EXAFS. Data were collected at the uranium L_{III}-edge (17.166 keV). Through a qualitative comparison with a complex of uranyl with benzamidoxime, the PAF-based adsorbents exhibited similar behavior (Figure S17). This is consistent with previous reports of open-chain amidoxime ligands binding to uranyl in a 2:1 fashion.[63] This preferential binding manner provides further evidence for the importance of the flexibility of PAF-1-NH$(CH_2)_2$AO. Comparing the maximum uptake capacities of PAF-1-CH_2NHAO (102 mg/g) and PAF-1-NH$(CH_2)_2$AO (385 mg/g), this is equivalent to uptakes of 0.43 and 1.62 mmol/g, respectively. Given the determined 2:1 binding with uranium, the corresponding ligand utilization are 0.86 and 3.24

DOI: 10.1021/acsami.9b09532
ACS Appl. Mater. Interfaces 2019, 11, 30919−30926

mmol/g, respectively. Taking into account the amidoxime content of the adsorbents, this results in PAF-1-CH_2NHAO only using 52% of the available ligands, wherein PAF-1-$NH(CH_2)_2$AO has near full utilization with a value of 96%. With an amorphous material, flexible ligands are beneficial to bind to a common uranyl ion, thus PAF-1-$NH(CH_2)_2$AO provides greater cooperation between neighboring functional groups resulting in an enhanced adsorption ability compared to PAF-1-CH_2NHAO.

CONCLUSIONS

Through the utilization of a stable and functional platform, PAF-1, changes in the amidoxime ligand were probed for the capture of uranium. Compared to PAF-1-CH_2NHAO, PAF-1-$NH(CH_2)_2$AO has enhanced cooperation between the neighboring amidoxime groups, resulting in a vastly improved uptake capacity and kinetic efficiency. PAF-1-$NH(CH_2)_2$AO demonstrates a high binding affinity for uranium, has the ability to be eluted and effectively recycled, and is able to recover uranium from the diverse composition of a spiked seawater solution. Given these promising results, it is evident that further exploration of the amidoxime group can produce an adsorbent material to economically recover uranium from seawater as a nuclear fuel source.

ASSOCIATED CONTENT

Supporting Information

The Supporting Information is available free of charge on the ACS Publications website at DOI: 10.1021/acsami.9b09532.

Full materials synthesis, uranium recovery efficiency, FT-IR spectra of intermediates and final product, nitrogen sorption isotherms of intermediates and final product, and X-ray absorption fine structure (XAFS) spectroscopy studies (PDF)

AUTHOR INFORMATION

Corresponding Author

*E-mail: sqma@usf.edu.

ORCID

Carter W. Abney: 0000-0002-1809-9577

Shengqian Ma: 0000-0002-1897-7069

Notes

The authors declare no competing financial interest.

ACKNOWLEDGMENTS

This work was supported by the DOE Office of Nuclear Energy's Nuclear Energy University Program (Grant No. DE-NE0008281). Partial support of this work came from the U.S. National Science Foundation (CBET-1706025) and the University of South Florida. MRCAT operations are supported by the Department of Energy and MRCAT member institutions. This research used resources of the Advanced Photon Source, a U.S. Department of Energy (DOE) Office of Science User Facility operated for the DOE Office of Science by Argonne National Laboratory under Contract No. DE-AC02-06CH11357. The authors acknowledge the help from Dr. Eric J. Werner at University of Tampa for use of the ICP-OES instrument.

REFERENCES

(1) Sholl, D. S.; Lively, R. P. Seven Chemical Separations to Change the World. *Nature* **2016**, *532*, 435−437.

(2) Sailor, W. C.; Bodansky, D.; Braun, C.; Fetter, S.; van der Zwaan, B. A Nuclear Solution to Climate Change? *Science* **2000**, *288*, 1177−1178.

(3) Sun, Q.; Aguila, B.; Ma, S. Opportunities of Porous Organic Polymers for Radionuclide Sequestration. *Trends Chem.* **2019**, *1*, 292−303.

(4) *Uranium 2016: Resources, Production and Demand; OECD Nuclear Energy Agency and the International Atomic Energy Agency, NEA#7301*, 2016.

(5) Lu, Y. Coordination Chemistry in the Ocean. *Nat. Chem.* **2014**, *6*, 175−177.

(6) Liu, C.; Hsu, P.-C.; Xie, J.; Zhao, J.; Wu, T.; Wang, H.; Liu, W.; Zhang, J.; Chu, S.; Cui, Y. A Half-Wave Rectified Alternating Current Electrochemical Method for Uranium Extraction from Seawater. *Nat. Energy* **2017**, *2*, No. 17007.

(7) Parker, B. F.; Zhang, Z.; Rao, L.; Arnold, J. An Overview and Recent Progress in the Chemistry of Uranium Extraction from Seawater. *Dalton Trans.* **2018**, *47*, 639−644.

(8) Sun, Q.; Aguila, B.; Perman, J.; Ivanov, A. S.; Bryantsev, V. S.; Earl, L. D.; Abney, C. W.; Wojtas, L.; Ma, S. Bio-Inspired Nano-Traps for Uranium Extraction from Seawater and Recovery from Nuclear Waste. *Nat. Commun.* **2018**, *9*, No. 1644.

(9) Yuan, Y.; Yang, Y.; Ma, X.; Meng, Q.; Wang, L.; Zhao, S.; Zhu, G. Molecularly Imprinted Porous Aromatic Frameworks and their Composite Components for Selective Extraction of Uranium Ions. *Adv. Mater.* **2018**, *30*, No. 1706507.

(10) Kim, J.; Tsouris, C.; Mayes, R. T.; Oyola, Y.; Saito, T.; Janke, C. J.; Dai, S.; Schneider, E.; Sachde, D. Recovery of Uranium from Seawater: A Review of Current Status and Future Research Needs. *Sep. Sci. Technol.* **2013**, *48*, 367−387.

(11) Wang, L. L.; Luo, F.; Dang, L. L.; Li, J. Q.; Wu, X. L.; Liu, S. J.; Luo, M. B. Ultrafast High-Performance Extraction of Uranium from Seawater without Pretreatment using an Acylamide- and Carboxyl-Functionalized Metal−Organic Framework. *J. Mater. Chem. A* **2015**, *3*, 13724−13730.

(12) Abney, C. W.; Mayes, R. T.; Saito, T.; Dai, S. Materials for the Recovery of Uranium from Seawater. *Chem. Rev.* **2017**, *117*, 13935−14013.

(13) Diallo, M. S.; Kotte, M. R.; Cho, M. Mining Critical Metals and Elements from Seawater: Opportunities and Challenges. *Environ. Sci. Technol.* **2015**, *49*, 9390−9399.

(14) Zhou, L.; Bosscher, M.; Zhang, C.; Öçubukçu, S.; Zhang, L.; Zhang, W.; Li, C. J.; Liu, J.; Jensen, M. P.; Lai, L.; He, C. A Protein Engineered to Bind Uranyl Selectively and with Femtomolar Affinity. *Nat. Chem.* **2014**, *6*, 236−241.

(15) Ivanov, A. S.; Parker, B. F.; Zhang, Z.; Aguila, B.; Sun, Q.; Ma, S.; Jansone-Popova, S.; Arnold, J.; Mayes, R. T.; Dai, S.; Bryantsev, V. S.; Rao, L.; Popovs, I. Siderophore-Inspired Chelator Hijacks Uranium from Aqueous Medium. *Nat. Commun.* **2019**, *10*, No. 819.

(16) Carboni, M.; Abney, C. W.; Taylor-Pashow, K. M. L.; Vivero-Escoto, J. L.; Lin, W. Uranium Sorption with Functionalized Mesoporous Carbon Materials. *Ind. Eng. Chem. Res.* **2013**, *52*, 15187−15197.

(17) Yang, X.; Li, J.; Liu, J.; Tian, Y.; Li, B.; Cao, K.; Liu, S.; Hou, M.; Li, S.; Ma, L. Simple Small Molecule Carbon Source Strategy for Synthesis of Functional Hydrothermal Carbon: Preparation of Highly Efficient Uranium Selective Solid Phase Extractant. *J. Mater. Chem. A* **2014**, *2*, 1550−1559.

(18) Tian, Y.; Fu, J.; Zhang, Y.; Cao, K.; Bai, C.; Wang, D.; Li, S.; Xue, Y.; Ma, L.; Zheng, C. Ligand-Exchange Mechanism: New Insight into Solid-Phase Extraction of Uranium based on a Combined Experimental and Theoretical Study. *Phys. Chem. Chem. Phys.* **2015**, *17*, 7214−7223.

(19) Zhang, Y.; Zhang, H.; Liu, Q.; Chen, R.; Liu, J.; Yu, J.; Jing, X.; Zhang, M.; Wang, J. Polypyrrole Modified Fe^0-Loaded Graphene

Oxide for the Enrichment of Uranium(VI) from Simulated Seawater. *Dalton Trans.* **2018**, *47*, 12984−12992.
(20) Alexandratos, S. D.; Zhu, X.; Florent, M.; Sellin, R. Polymer-Supported Bifunctional Amidoximes for the Sorption of Uranium from Seawater. *Ind. Eng. Chem. Res.* **2016**, *55*, 4208−4216.
(21) Xie, S.; Liu, X.; Zhang, B.; Ma, H.; Ling, C.; Yu, M.; Li, L.; Li, J. Electrospun Nanofibrous Adsorbents for Uranium Extraction from Seawater. *J. Mater. Chem. A* **2015**, *3*, 2552−2558.
(22) Carboni, M.; Abney, C. W.; Liu, S.; Lin, W. Highly Porous and Stable Metal−Organic Frameworks for Uranium Extraction. *Chem. Sci.* **2013**, *4*, 2396−2402.
(23) Chen, L.; Bai, Z.; Zhu, L.; Zhang, L.; Cai, Y.; Li, Y.; Liu, W.; Wang, Y.; Chen, L.; Diwu, J.; Wang, J.; Chai, Z.; Wang, S. Ultrafast and Efficient Extraction of Uranium from Seawater Using an Amidoxime Appended Metal−Organic Framework. *ACS Appl. Mater. Interfaces* **2017**, *9*, 32446−32451.
(24) Ma, S.; Huang, L.; Ma, L.; Shim, Y.; Islam, S. M.; Wang, P.; Zhao, L.-D.; Wang, S.; Sun, G.; Yang, X.; Kanatzidis, M. G. Efficient Uranium Capture by Polysulfide/Layered Double Hydroxide Composites. *J. Am. Chem. Soc.* **2015**, *137*, 3670−3677.
(25) Manos, M. J.; Kanatzidis, M. G. Layered Metal Sulfides Capture Uranium from Seawater. *J. Am. Chem. Soc.* **2012**, *134*, 16441−16446.
(26) Sun, Q.; Dai, Z.; Meng, X.; Xiao, F.-S. Porous Polymer Catalysts with Hierarchical Structures. *Chem. Soc. Rev.* **2015**, *44*, 6018−6034.
(27) Tan, L.; Tan, B. Hypercrosslinked Porous Polymer Materials: Design, Synthesis, and Applications. *Chem. Soc. Rev.* **2017**, *46*, 3322−3356.
(28) Slater, A. G.; Cooper, A. I. Function-Led Design of New Porous Materials. *Science* **2015**, *348*, No. aaa8075.
(29) Xu, Y.; Jin, S.; Xu, H.; Nagai, A.; Jiang, D. Conjugated Microporous Polymers: Design, Synthesis and Application. *Chem. Soc. Rev.* **2013**, *42*, 8012−8031.
(30) Das, S.; Heasman, P.; Ben, T.; Qiu, S. Porous Organic Materials: Strategic Design and Structure−Function Correlation. *Chem. Rev.* **2017**, *117*, 1515−1563.
(31) Alsbaiee, A.; Smith, B. J.; Xiao, L.; Ling, Y.; Helbling, D. E.; Dichtel, W. R. Rapid Removal of Organic Micropollutants from Water by a Porous β-Cyclodextrin Polymer. *Nature* **2016**, *529*, 190−194.
(32) Furukawa, H.; Cordova, K. E.; O'Keeffe, M.; Yaghi, O. M. The Chemistry and Applications of Metal-Organic Frameworks. *Science* **2013**, *341*, No. 1230444.
(33) Howarth, A. J.; Peters, A. W.; Vermeulen, N. A.; Wang, T. C.; Hupp, J. T.; Farha, O. K. Best Practices for the Synthesis, Activation, and Characterization of Metal−Organic Frameworks. *Chem. Mater.* **2017**, *29*, 26−39.
(34) Perrich, J. R. *Activated Carbon Adsorption for Wastewater Treatment*; CRC Press, 2018.
(35) Sun, Q.; Zhu, L.; Aguila, B.; Thallapally, P. K.; Xu, C.; Chen, J.; Wang, S.; Rogers, D.; Ma, S. Optimizing Radionuclide Sequestration in Anion Nanotraps with Record Pertechnetate Sorption. *Nat. Commun.* **2019**, *10*, No. 1646.
(36) Aguila, B.; Sun, Q.; Perman, J. A.; Earl, L. D.; Abney, C. W.; Elzein, R.; Schlaf, R.; Ma, S. Efficient Mercury Capture Using Functionalized Porous Organic Polymer. *Adv. Mater.* **2017**, *29*, No. 1700665.
(37) Ben, T.; Ren, H.; Ma, S.; Cao, D.; Lan, J.; Jing, X.; Wang, W.; Xu, J.; Deng, F.; Simmons, J. M.; Qiu, S.; Zhu, G. Targeted Synthesis of a Porous Aromatic Framework with High Stability and Exceptionally High Surface Area. *Angew. Chem., Int. Ed.* **2009**, *48*, 9457−9460.
(38) Demir, S.; Brune, N. K.; Van Humbeck, J. F.; Mason, J. A.; Plakhova, T. V.; Wang, S.; Tian, G.; Minasian, S. G.; Tyliszczak, T.; Yaita, T.; Kobayashi, T.; Kalmykov, S. N.; Shiwaku, H.; Shuh, D. K.; Long, J. R. Extraction of Lanthanide and Actinide Ions from Aqueous Mixtures Using a Carboxylic Acid-Functionalized Porous Aromatic Framework. *ACS. Cent. Sci.* **2016**, *2*, 253−265.
(39) Li, B.; Zhang, Y.; Ma, D.; Xing, Z.; Ma, T.; Shi, Z.; Ji, X.; Ma, S. Creation of a New Type of Ion Exchange Material for Rapid, High-Capacity, Reversible and Selective Ion Exchange without Swelling and Entrainment. *Chem. Sci.* **2016**, *7*, 2138−2144.
(40) Li, B.; Zhang, Y.; Ma, D.; Shi, Z.; Ma, S. Mercury Nano-Trap for Effective and Efficient Removal of Mercury(II) from Aqueous Solution. *Nat. Commun.* **2014**, *5*, No. 5537.
(41) Li, B.; Sun, Q.; Zhang, Y.; Abney, C. W.; Aguila, B.; Lin, W.; Ma, S. Functionalized Porous Aromatic Framework for Efficient Uranium Adsorption from Aqueous Solutions. *ACS Appl. Mater. Interfaces* **2017**, *9*, 12511−12517.
(42) Sun, Q.; Aguila, B.; Earl, L. D.; Abney, C. W.; Wojtas, L.; Thallapally, P. K.; Ma, S. Covalent Organic Frameworks as a Decorating Platform for Utilization and Affinity Enhancement of Chelating Sites for Radionuclide Sequestration. *Adv. Mater.* **2018**, *30*, No. 1705479.
(43) Kelley, S. P.; Barber, P. S.; Mullins, P. H. K.; Rogers, R. D. Structural Clues to UO_2^{2+}/VO_2^{+} Competition in Seawater Extraction Using Amidoxime-Based Extractants. *Chem. Commun.* **2014**, *50*, 12504−12507.
(44) Zhang, A.; Asakura, T.; Uchiyama, G. The Adsorption Mechanism of Uranium(VI) from Seawater on a Macroporous Fibrous Polymeric Adsorbent Containing Amidoxime Chelating Functional Group. *React. Funct. Polym.* **2003**, *57*, 67−76.
(45) Abney, C. W.; Mayes, R. T.; Piechowicz, M.; Lin, Z.; Bryantsev, V. S.; Veith, G. M.; Dai, S.; Lin, W. XAFS Investigation of Polyamidoxime-Bound Uranyl Contests the Paradigm from Small Molecule Studies. *Energy Environ. Sci.* **2016**, *9*, 448−453.
(46) Vukovic, S.; Watson, L. A.; Kang, S. O.; Custelcean, R.; Hay, B. P. How Amidoximate Binds the Uranyl Cation. *Inorg. Chem.* **2012**, *51*, 3855−3859.
(47) Zhang, A.; Uchiyama, G.; Asakura, T. pH Effect on the Uranium Adsorption from Seawater by a Macroporous Fibrous Polymeric Material Containing Amidoxime Chelating Functional Group. *React. Funct. Polym.* **2005**, *63*, 143−153.
(48) Barber, P. S.; Kelley, S. P.; Rogers, R. D. Highly Selective Extraction of the Uranyl Ion with Hydrophobic Amidoxime-Functionalized Ionic Liquids via η^2 Coordination. *RSC Adv.* **2012**, *2*, 8526−8530.
(49) Kawakami, T.; Akiyama, E.; Hori, K.; Nagase, Y.; Sugo, T. Structural Changes of Compounds Containing Cyano Groups by Hydroxylamine Treatment. *Trans. Mater. Res. Soc. Jpn.* **2002**, *27*, 783−786.
(50) Lowell, S.; Shields, J. E. *Powder Surface Area and Porosity*; Springer Science & Business Media, 2013.
(51) Langmuir, I. The Constitution and Fundamental Properties of Solids and Liquids. Part I. Solids. *J. Am. Chem. Soc.* **1916**, *38*, 2221−2295.
(52) Krupka, K.; Kaplan, D.; Whelan, G.; Serne, R.; Mattigod, S. Understanding Variation in Partition Coefficient, K_d, Values. *The K_d Model, Methods of Measurement, and Application of Chemical Reaction Codes*; US Environmental Protection Agency: Washington, DC, 1999; Vol. *1*.
(53) Park, I.-H.; Suh, J.-M. Preparation and Uranyl Ion Adsorptivity of Macroreticular Chelating Resins Containing a Pair of Neighboring Amidoxime Groups in a Monomeric Styrene Unit. *Angew. Makromol. Chem.* **1996**, *239*, 121−132.
(54) Tripathi, A.; Melo, J. S. Synthesis of a Low-Density Biopolymeric Chitosan−Agarose Cryomatrix and its Surface Functionalization with Bio-Transformed Melanin for the Enhanced Recovery of Uranium(VI) from Aqueous Subsurfaces. *RSC Adv.* **2016**, *6*, 37067−37078.
(55) Yang, P.; Liu, Q.; Liu, J.; Zhang, H.; Li, Z.; Li, R.; Liu, L.; Wang, J. Interfacial Growth of a Metal−Organic Framework (UiO-66) on Functionalized Graphene Oxide (GO) as a Suitable Seawater Adsorbent for Extraction of Uranium(VI). *J. Mater. Chem. A* **2017**, *5*, 17933−17942.
(56) Wang, D.; Song, J.; Wen, J.; Yuan, Y.; Liu, Z.; Lin, S.; Wang, H.; Wang, H.; Zhao, S.; Zhao, X.; Fang, M.; Lei, M.; Li, B.; Wang, N.; Wang, X.; Wu, H. Significantly Enhanced Uranium Extraction from

DOI: 10.1021/acsami.9b09532
ACS Appl. Mater. Interfaces 2019, 11, 30919−30926

Seawater with Mass Produced Fully Amidoximated Nanofiber Adsorbent. *Adv. Energy Mater.* **2018**, *8*, No. 1802607.
(57) Huang, L.; Zhang, L.; Hua, D. Synthesis of Polyamidoxime-Functionalized Nanoparticles for Uranium(IV) Removal from Neutral Aqueous Solutions. *J. Radioanal. Nucl. Chem.* **2015**, *305*, 445−453.
(58) Zhou, S.; Chen, B.; Li, Y.; Guo, J.; Cai, X.; Qin, Z.; Bai, J.; Na, P. Synthesis, Characterization, Thermodynamic and Kinetic Investigations on Uranium (VI) Adsorption using Organic-Inorganic Composites: Zirconyl-Molybdopyrophosphate-Tributyl Phosphate. *Sci. China Chem.* **2013**, *56*, 1516−1524.
(59) Li, D.; Egodawatte, S.; Kaplan, D. I.; Larsen, S. C.; Serkiz, S. M.; Seaman, J. C.; Scheckel, K. G.; Lin, J.; Pan, Y. Sequestration of U(VI) from Acidic, Alkaline, and High Ionic-Strength Aqueous Media by Functionalized Magnetic Mesoporous Silica Nanoparticles: Capacity and Binding Mechanisms. *Environ. Sci. Technol.* **2017**, *51*, 14330−14341.
(60) Deane, A. M.; Richards, E. W. T.; Stephen, I. G. Bond Orientations in Uranyl Nitrate Hexahydrate Using Attenuated Total Reflection. *Spectrochim. Acta* **1966**, *22*, 1253−1260.
(61) Amayri, S.; Arnold, T.; Reich, T.; Foerstendorf, H.; Geipel, G.; Bernhard, G.; Massanek, A. Spectroscopic Characterization of the Uranium Carbonate Andersonite $Na_2Ca[UO_2(CO_3)_3]\cdot 6H_2O$. *Environ. Sci. Technol.* **2004**, *38*, 6032−6036.
(62) Mosquera, A. A.; Horwat, D.; Rashkovskiy, A.; Kovalev, A.; Miska, P.; Wainstein, D.; Albella, J. M.; Endrino, J. L. Exciton and Core-Level Electron Confinement Effects in Transparent ZnO Thin Films. *Sci. Rep.* **2013**, *3*, No. 1714.
(63) Ladshaw, A. P.; Ivanov, A. S.; Das, S.; Bryantsev, V. S.; Tsouris, C.; Yiacoumi, S. First-Principles Integrated Modeling for Selective Capture of Uranium from Seawater by Polyamidoxime Sorbent Materials. *ACS Appl. Mater. Interfaces* **2018**, *10*, 12580−12593.

DOI: 10.1021/acsami.9b09532
ACS Appl. Mater. Interfaces 2019, 11, 30919−30926